



**HAL**  
open science

## Analysis, rigorous design and characterization of a three-layer anisotropic transmitarray at 300 GHz

Orestis Koutsos, Francesco Manzillo, Antonio Clemente, Ronan Sauleau

### ► To cite this version:

Orestis Koutsos, Francesco Manzillo, Antonio Clemente, Ronan Sauleau. Analysis, rigorous design and characterization of a three-layer anisotropic transmitarray at 300 GHz. *IEEE Transactions on Antennas and Propagation*, 2022, 70 (7), pp.5437-5446. 10.1109/TAP.2022.3145506 . cea-03637103

**HAL Id: cea-03637103**

**<https://cea.hal.science/cea-03637103>**

Submitted on 11 Apr 2022

**HAL** is a multi-disciplinary open access archive for the deposit and dissemination of scientific research documents, whether they are published or not. The documents may come from teaching and research institutions in France or abroad, or from public or private research centers.

L'archive ouverte pluridisciplinaire **HAL**, est destinée au dépôt et à la diffusion de documents scientifiques de niveau recherche, publiés ou non, émanant des établissements d'enseignement et de recherche français ou étrangers, des laboratoires publics ou privés.

# Analysis, Rigorous Design and Characterization of a Three-layer Anisotropic Transmitarray at 300 GHz

Orestis Koutsos, Francesco Foglia Manzillo, *Member, IEEE*, Antonio Clemente, *Senior Member, IEEE* and Ronan Sauleau, *Fellow, IEEE*

**Abstract**—A novel approach for studying and designing low-cost anisotropic transmitarrays at sub-THz frequencies is presented here. The array comprises three metal layers and two interleaved dielectric spacers. A four-port equivalent circuit model is derived to accurately model the anisotropic behavior of the unit-cell. The analysis proves theoretically that nearly perfect transmission and complete phase control can be achieved at the same time. A systematic procedure optimizing the admittance tensor of the inner layer is described for the unit-cell design. A 3-bit transmitarray antenna at 300 GHz is fabricated using a standard printed circuit board process. The measured results demonstrate that the design methodology is effective even under strict technological constraints. The antenna achieves a peak gain of 32.2 dBi with 36.5% aperture efficiency and 70.4 GHz of 3-dB bandwidth.

**Index Terms**—transmitarray, anisotropy, equivalent circuit, periodic structures, 300 GHz, sub-THz, admittance tensor.

## I. INTRODUCTION

THE use of currently unexploited spectrum around 300 GHz could be a key enabler for the deployment of next-generation wireless communication systems. At these frequencies, the main challenge is to mitigate the high propagation losses by realizing high-gain, efficient and wideband antennas. In addition, the choice of the fabrication process is crucial for the final performance, due to the small design features, as well as for enabling low-cost solutions.

Among the existing architectures that are suitable for sub-THz applications, transmitarray (TA) antennas are one of the best candidates. In particular, they do not require lossy feed networks, thanks to the spatial feeding mechanism. On top of that, TAs do not suffer from feed blockage, which makes them suitable for near-field excitation. Moreover, the fabrication of TAs is compatible with low-cost planar processes. These characteristics enable the design of a cost-efficient, low-profile antenna with high aperture efficiency and beamforming capabilities in the sub-THz region.

Manuscript received XXXXX XX, XXXX; revised XXXX XX, XXXX; accepted XXXXX XX, XXXX. This work was partly supported by the National Research Agency (ANR) through the project “Next5G” under Grant ANR 18-CEA25-0009-01.

O. Koutsos is with Univ. Grenoble Alpes, CEA, Leti, F-38000 Grenoble, France, and also with Univ Rennes, CNRS, Institut d’Électronique et des Technologies du numéRique (IETR) - UMR 6164, F-35000 Rennes, France (e-mail: orestis.koutsos@cea.fr).

F. Foglia Manzillo and A. Clemente are with Univ. Grenoble Alpes, CEA, Leti, F-38000 Grenoble, France (e-mail: antonio.clemente@cea.fr; francesco.fogliamanzillo@cea.fr).

R. Sauleau is with Univ Rennes, CNRS, Institut d’Électronique et des Technologies du numéRique (IETR) - UMR 6164, F-35000 Rennes, France (e-mail: ronan.sauleau@univ-rennes1.fr).

The key to achieve high performance is the selection of convenient unit-cell (UC) designs and the capability to rigorously control and tune their electromagnetic properties. At frequencies below 100 GHz, the most common UC architecture is the antenna-filter-antenna (AFA). It generally comprises two antenna elements physically connected using a metallized via, e.g. [1], [2]. However, at sub-THz frequencies, the fabrication constraints hinder the achievement of optimal UC performance. To cope with this problem, a hybrid design approach was presented at D-band [3]. The authors combined AFA unit-cells comprising either vias- or aperture-coupled radiating elements and demonstrated a 3-bit TA. Nevertheless, at even higher frequencies, this design methodology can not overcome the technological limitations of low-cost processes, e.g. Printed Circuit Board (PCB), especially when a high phase resolution is targeted ( $> 2$ -bit). Furthermore, the strong impact on the metallized via diameter and alignment, which lead to a frequency shift of about 5 GHz (3.6% at 140 GHz) in [3], can be mitigated using a vias-less design.

Alternative designs rely on frequency-selective surfaces (FSS). The unit-cells are via-less and comprise multiple metal layers, separated by air gap or dielectric spacers [4]–[7]. In most cases, each sheet impedance is isotropic. However, anisotropic designs can offer enhanced performance and functionalities. The UC presented in [8]–[12] achieves high efficiency over wide bandwidth using only three metal layers: two orthogonal polarization grids and an inner polarization rotator. This design was originally proposed as a  $90^\circ$  polarization converter at optical frequencies [13]–[15]. Furthermore, by optimizing only the middle layer, phase-shifting surfaces for wavefront manipulation and TA antennas with high phase resolution can be realized. Recently, several TA designs have been demonstrated using this concept up to 300 GHz [16]–[18].

Despite the increasing number of TAs based on similar architectures, to the best of authors’ knowledge, no theoretical approaches for the analysis and synthesis of these elements have been presented. In most cases, a large number of parameters (e.g. geometrical features and material properties) has to be simultaneously optimized, for each phase-shifting UC, with the only objective of achieving a target insertion loss. This blind parametric process does not provide any insight on the design of the optimal UC and it becomes less efficient as the TA phase resolution increases. Therefore, the procedure can be time-consuming and does not guarantee to reach the maximum achievable performance.

In this paper, we present a rigorous model based on cas-

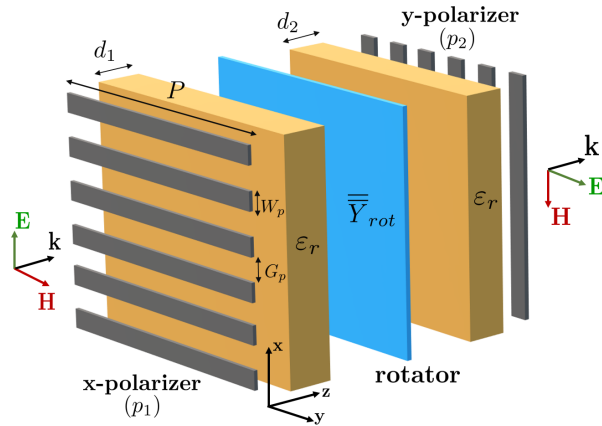


Fig. 1: Exploded view of the proposed unit-cell with  $P$  periodicity, which is the same along the  $x$ - and  $y$ -axis. The rotator (blue color) is generically modelled as a two-dimensional sheet impedance described by a  $2 \times 2$  admittance matrix. The polarization grids (grey color) are orthogonally oriented. The layers are interleaved by two dielectric spacers (orange color) of the same permittivity,  $\epsilon_r$ .

caded sheet admittances [19] to analyze and synthesize this class of unit-cells, with application to TA antennas. Some preliminary results have been presented in part in our previous works [18] and [20], describing the UC operation principle and focusing only on the design of the inner metal layer. Here, in addition to the fabrication and experimental characterization of a prototype, a more general analysis of the UC and a quantitative procedure to design it for maximum transmission and phase coverage are thoroughly described. Furthermore, the theoretical model and the design methodology are augmented by the use of a four-port equivalent circuit to take into account the UC anisotropy. Thanks to this circuit model, a general closed-form expression for the transmission coefficient of the UC is presented for the first time. The analysis presented in Section II shows that the anisotropy enables full phase coverage with very small insertion loss, as opposed to three-layer isotropic UCs [21]. The synthesis procedure, described in Section III, provides the optimal admittance tensor of the polarization rotator, expressed in a convenient reference system, easing the UC design. In the same Section, an in-depth study of the impact of the grid polarizers and the dielectric spacers on the insertion loss and bandwidth is presented. To validate this procedure, a 3-bit TA antenna is fabricated using a standard PCB technology and characterized at 300 GHz. As presented in Section IV, the prototype achieves high gain and aperture efficiency over a 25% relative bandwidth. Finally, conclusions are drawn in Section V.

## II. UNIT-CELL ANALYSIS

### A. Circuit Model

A general view of the proposed unit-cell is shown in Fig.1. The structure is periodic in the  $xy$ -plane and it comprises three metallic layers [18]. The outer layers are two orthogonal polarization grids, which are assumed identical. The inner layer is an anisotropic sheet that modifies the polarization of a wave impinging on the cell. This sheet is interleaved by two

dielectric spacers of permittivity  $\epsilon_r$  and thicknesses  $d_1$  and  $d_2$ , respectively. Finally, in this study all materials are considered lossless, homogeneous, isotropic and non-dispersive.

The unit-cell is illuminated in either side by a plane wave,  $x$ - or  $y$ -polarized, propagating along the  $z$ -axis. As presented in Fig. 1, the structure rotates by  $90^\circ$  the polarization of the incident wave. The complete scattering phenomenon is modelled by the equivalent circuit of Fig. 2, assuming normal incidence. The employment of a four-port network is necessary in order to take into account the mode coupling induced by the rotator. The spacers are modelled as transmission lines, and for normal incidence the characteristic impedance will be the same for each polarization. Therefore, the characteristic impedances of the spacers are  $Z_{\epsilon_r}^x = Z_{\epsilon_r}^y = \eta_0 / \sqrt{\epsilon_r}$ , where  $\eta_0$  is the free space impedance, and all the ports have the same generator impedance  $Z_0^x = Z_0^y = Z_0$ . For simplicity, the medium surrounding the unit-cell is assumed to be vacuum ( $Z_0 = \eta_0$ ). Due to the periodical nature of the problem, the circuit representation is accurate when only the dominant mode of the Floquet Waves (FWs) is propagating within the frequency range of observation. Furthermore, the circuit does not take into account coupling effects among stacked layers. These assumptions depend on both period and frequency, which can be validated through full-wave simulations. Therefore, in order to obtain accurate results using this model, separations greater than  $\lambda/8$  between the layers must be considered and the periodicity of each layer should be equal or less than  $\lambda/2$  at the highest operating frequency.

The polarizers act as reflective or transparent surfaces to orthogonal linearly-polarized incident fields. The strip grating has been thoroughly studied previously, e.g. [22]–[25]. Here, it is assumed that the grid has sub-wavelength periodicity and is placed so that the transmitted and reflected fields are parallel to the  $x$ - and  $y$ -axis, respectively. Therefore, each grid is seen as a couple of shunt admittances,  $Y_p^x$  and  $Y_p^y$ , loading the corresponding transmission lines. Since the two polarizers are considered identical, these parameters are

$$Y_{p1}^x = Y_{p2}^y = Y_t, \quad (1a)$$

$$Y_{p1}^y = Y_{p2}^x = Y_r. \quad (1b)$$

The value  $Y_t$  describes the case of transparency and the value  $Y_r$  describes the case of reflection. In general, it is known that  $Y_t$  and  $Y_r$  exhibit a small capacitive and a finite inductive value, respectively. Nevertheless, in many studies the polarizers are assumed ideal, in order to exploit the polarization properties and simplify the analysis. In that case, the respective values will be

$$Y_t = 0, \quad (2a)$$

$$Y_r \rightarrow -\infty. \quad (2b)$$

The equivalent circuit of Fig. 2 as well as most results presented in this work are valid for any admittance values of the outer layers. Nevertheless, the above approximation can be used to derive a simple analytical expression of the transmission coefficient.

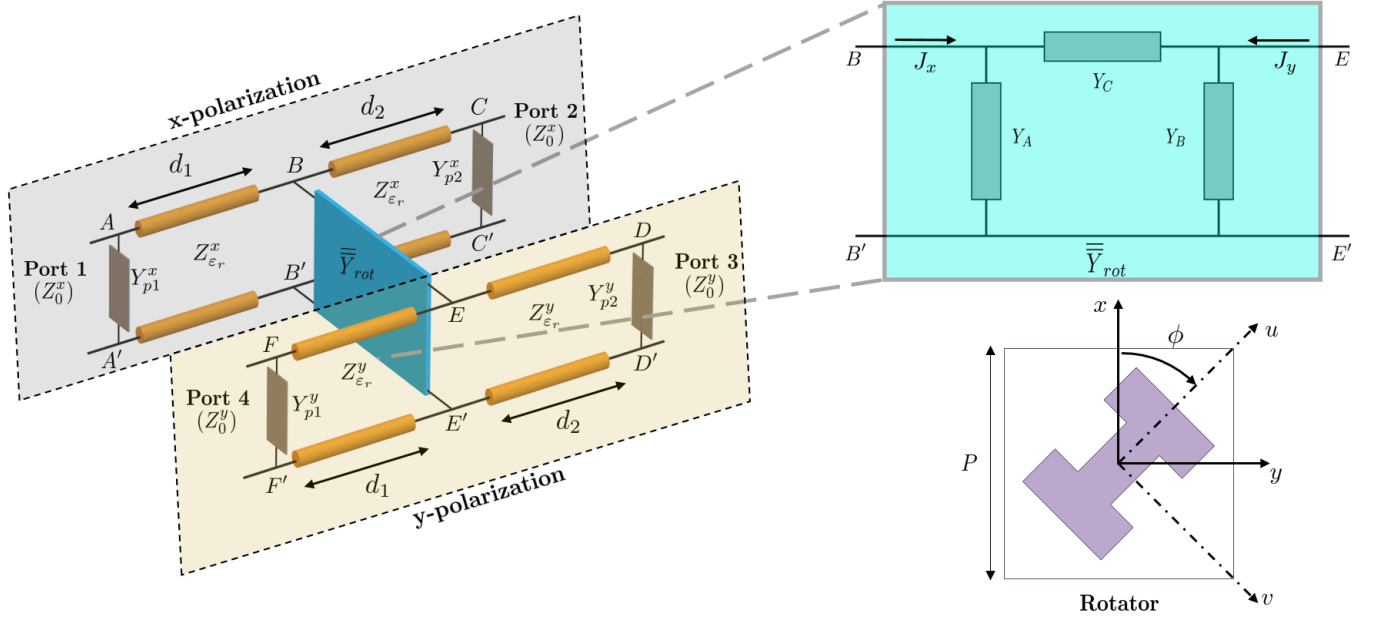


Fig. 2: Equivalent four-port circuit of the unit-cell. Both polarizers,  $p_1$  and  $p_2$ , are represented as a pair of shunt admittances at the ends of  $x$  and  $y$  transmission lines, respectively. The rotator is modelled by a  $\pi$ -type network, coupling the two transmission lines at  $BB'$  and  $EE'$ . A rotator design and the reference systems necessary to illustrate the diagonalization of  $\bar{\bar{Y}}_{rot}$  are shown in the bottom right corner.

The rotator is coupling the two polarizations in the  $(x, y)$  system. The anisotropic behavior of this layer can be described by a  $2 \times 2$  admittance tensor given by

$$\bar{\bar{Y}}_{rot} = \begin{bmatrix} Y_{xx} & Y_{xy} \\ Y_{yx} & Y_{yy} \end{bmatrix} \quad (3)$$

The entries  $Y_{xy}$  and  $Y_{yx}$  represent the polarization coupling and they are equal by reciprocity. The tensor  $\bar{\bar{Y}}_{rot}$  relates the components of the surface current,  $J_x$  and  $J_y$ , to the average electric field components across the rotator sheet [19], [26]. This relationship can be represented by a  $\pi$ -type circuit [27], placed between the  $x$  and  $y$  transmission lines, as shown in Fig. 2. The values of the admittances of the  $\pi$ -network are

$$Y_A = Y_{xx} + Y_{xy} \quad (4a)$$

$$Y_B = Y_{yy} + Y_{xy} \quad (4b)$$

$$Y_C = -Y_{xy} \quad (4c)$$

Consequently, the overall unit-cell is modelled using five admittance values, namely  $Y_{xx}$ ,  $Y_{yy}$ ,  $Y_{xy}$ ,  $Y_t$  and  $Y_r$ . Considering the circuit of Fig. 2, the main objective is to calculate the scattering coefficient  $S_{31}$ , which will be referred to as  $T^{yx}$  in the rest of the paper, maximize its amplitude and tune its phase. Based on the classical network analysis [27], the general expression of this transmission coefficient is calculated as

$$S_{31} \triangleq T^{yx} = (Z_{AA'}^{-1} - Y_t)(1 + S_{11})K_1K_2^{-1}. \quad (5)$$

The expressions  $K_1$  and  $K_2$  are given in the appendix. The value  $Z_{AA'}$  is the equivalent input impedance at Port 1 when all other ports are terminated by a matched load ( $Z_0$ ). The value  $S_{11}$  is the reflection coefficient at Port 1; it is equal to

$$S_{11} = \frac{Z_{AA'} - Z_0}{Z_{AA'} + Z_0} \quad (6)$$

If the properties of the polarizers and the spacers are known, then the expression (5) is a function of the three admittance entries of the rotator. Although in this case the unit-cell can be studied and optimized focusing only on the inner sheet, the analysis remains somewhat complicated. In addition, the synthesis of the admittance tensor and the physical design of the rotator are still problematic, especially due to the coupling factor  $Y_{xy}$ , which is hard to control. Therefore, a convenient expression for the admittance tensor is found by applying a coordinate transformation [28]. In particular, the tensor  $\bar{\bar{Y}}_{rot}$  is diagonal in the  $(u, v)$  reference system, which is called crystal system and it exists for any passive two-dimensional structure [29]. It can be obtained by rotating the  $(x, y)$  system by an angle  $\phi$ , as shown in Fig. 2. The following relationship holds

$$\bar{\bar{Y}}_{rot}^{XY} = \bar{\bar{R}}(\phi)\bar{\bar{Y}}_{rot}^{UV}\bar{\bar{R}}^T(\phi), \quad (7)$$

where  $\bar{\bar{R}}(\phi)$  is the rotation matrix and the superscripts  $XY$  and  $UV$  indicate the two reference systems. The diagonalized matrix is

$$\bar{\bar{Y}}_{rot}^{UV} = \begin{bmatrix} Y_u & 0 \\ 0 & Y_v \end{bmatrix} \quad (8)$$

The three original entries of the rotator admittance can be expressed in terms of the two entries of the diagonalized matrix, yielding

$$Y_{xx} = \cos^2(\phi)Y_u + \sin^2(\phi)Y_v, \quad (9a)$$

$$Y_{yy} = \sin^2(\phi)Y_u + \cos^2(\phi)Y_v, \quad (9b)$$

$$Y_{xy} = \sin(\phi)\cos(\phi)(Y_u - Y_v). \quad (9c)$$

The entries  $Y_u$  and  $Y_v$  can be determined from the scattering parameters of the rotator sheet under  $u$ - and  $v$ -polarized fields. In particular, by simulating the rotator sheet with periodic

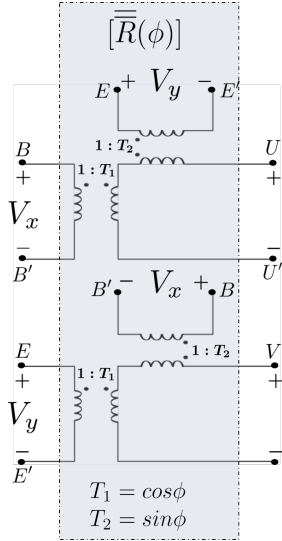


Fig. 3: Equivalent circuit of the rotation matrix, describing the relationship between the electric field components in the two coordinate systems. Ideal transformers are considered for the angle of rotation. The transpose rotation matrix is modelled by a similar network.

boundaries at the interface between two semi-infinite media of characteristic impedance  $\eta = \eta_0/\sqrt{\epsilon_r}$ , the expressions for the admittances are [27]

$$Y_{u,v} = -\frac{2S_{11}^{u,v}}{\eta(1+S_{11}^{u,v})}, \quad (10)$$

where  $S_{11}^{u,v}$  is the reflection coefficient at each polarization. Therefore, the admittance parameters are expressed in the  $(x,y)$  system as a function of  $Y_u$ ,  $Y_v$  and  $\phi$ . The circuit representation of the proposed transformation is shown in Fig. 3. The rotation matrix is illustrated using ideal transformers, in order to describe the relationship between the electric field components in the two coordinate systems. Therefore, the  $\pi$ -circuit in Fig. 2 can be replaced by the circuit of the rotation matrix and its transpose, placing between them the shunt admittances  $Y_u$  and  $Y_v$ .

The impact of the angle of rotation can be studied by focusing on the properties of depolarization of the rotator. It was shown in our previous work [20] that if  $\phi = \pm 45^\circ$ , the rotator achieves maximum polarization conversion. For this angle of rotation, the three entries of the  $\pi$ -circuit in (4) become

$$Y_A = Y_B = \begin{cases} Y_u, & \text{if } \phi = 45^\circ, \\ Y_v, & \text{if } \phi = -45^\circ, \end{cases} \quad (11a)$$

$$Y_C = \pm(Y_v - Y_u)/2, \text{ for } \phi = \pm 45^\circ. \quad (11b)$$

Therefore, thanks to the transformation concept, the unit-cell can be analyzed using four admittances,  $Y_u$ ,  $Y_v$ ,  $Y_t$  and  $Y_r$ , instead of five. Finally, the value  $Y_{xy}$  vanishes and thus, by fixing the rest of the parameters, expression (5) can be completely described only by the two values,  $Y_u$  and  $Y_v$ , which are related to the rotator in the crystal system.

### B. Transmission Phase Coverage

To demonstrate the effectiveness of the model for TA design, the unit-cell is examined in terms of phase coverage. Based on

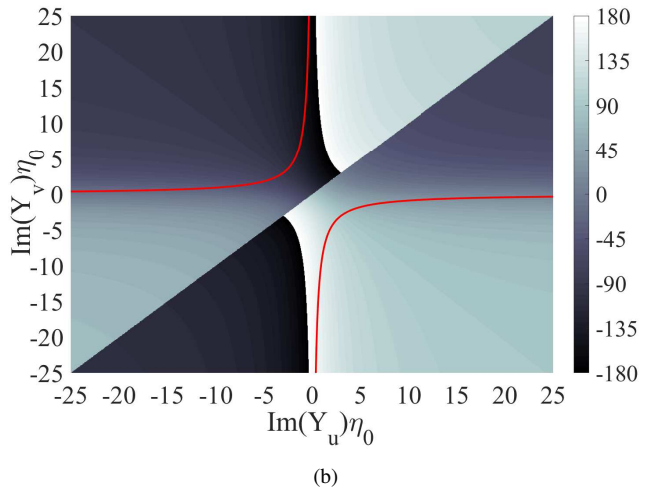
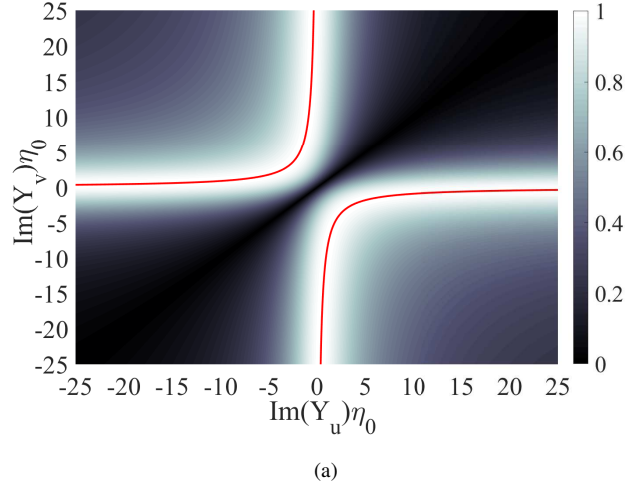


Fig. 4: Magnitude (a) and phase (b) of  $T^{yx}$  as function of the rotator admittance entries calculated at the crystal axes. The polarizers are assumed ideal and both spacers have a thickness of  $\lambda/4$ . The results are obtained using (12) for  $\phi = 45^\circ$ . The red solid curve in both figures represents the locus corresponding to perfect transmission, derived from (13).

the circuit theory, the objective is to calculate the impedance matching condition (IMC) in order to maximize the power transfer from Port 1 to Port 3. After that, the phase of transmission will be studied considering either zero or very low insertion loss (IL).

First, quarter-wavelength spacers are considered, i.e.  $d_1 = d_2 = \lambda/4$ , where  $\lambda = \lambda_0/\sqrt{\epsilon_r}$ , in order to derive a simple closed-form formula for the transmission coefficient. It will be shown in Section III that using a thickness close to this value, both wide bandwidth and low insertion loss can be achieved. Furthermore, the two polarizers are assumed ideal using (2) and thus a total reflection occurs at ports 2 and 4. Under these assumptions and choosing  $\phi = \pm 45^\circ$ , expression (5) yields

$$T^{yx} = \pm \frac{(Y_v - Y_u)\epsilon_r Z_0}{\epsilon_r^2 + Y_u Y_v Z_0^2 + (Y_u + Y_v)\epsilon_r Z_0} \quad (12)$$

The magnitude and phase of (12) are plotted in Fig. 4 a a function of  $Y_u$  and  $Y_v$ . Assuming lossless materials, each

admittance is described by a susceptance. Solving (12) for perfect transmission, the following locus is obtained

$$Y_u Y_v = (\epsilon_r / Z_0)^2. \quad (13)$$

As long as the admittance values are defined by (13), the unit-cell will exhibit zero insertion loss and cover the whole phase range, from  $-180^\circ$  to  $180^\circ$ . This shows that the anisotropy of the cell can improve the performance for TA design, compared to three-layer designs comprising symmetric FSS, which, instead, cannot cover the full phase range achieving perfect transmission [21]. Another interesting observation is that the IMC is satisfied only when  $\phi = \pm 45^\circ$ . When  $\phi \neq \pm 45^\circ$ , the behavior of transmission is similar, but the maximum magnitude becomes smaller than one. Lastly, in order to satisfy (13), the rotator must exhibit purely capacitive and purely inductive properties for each polarization, respectively, along the crystal axes.

Similar conclusions can be drawn when the two spacers exhibit the same thickness but not equal to  $\lambda/4$ . In particular, if (5) is solved for perfect transmission when  $d_1 = d_2 = d$ , a similar locus is derived. Specifically, the expression defines a hyperbola whose vertices are shifted toward the line  $Y_u = Y_v$  as a function of the thickness and the permittivity. For  $\epsilon_r = 1$ , the locus is simplified to

$$(Y_u - jZ_0^{-1} \cot(\beta_0 d))(Y_v - jZ_0^{-1} \cot(\beta_0 d)) = (1/Z_0)^2, \quad (14)$$

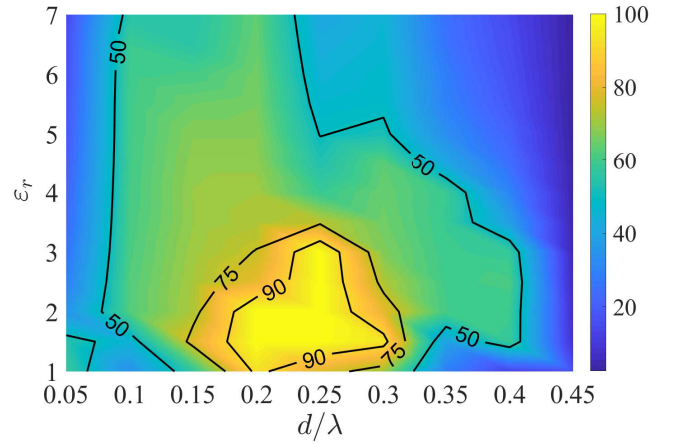
where  $\beta_0 = 2\pi/\lambda_0$ . Finally, when  $d = n\lambda/2$ , with  $n \in \mathbb{N}$ , the problem has no solution and the transmission is zero.

### III. UNIT-CELL SYNTHESIS

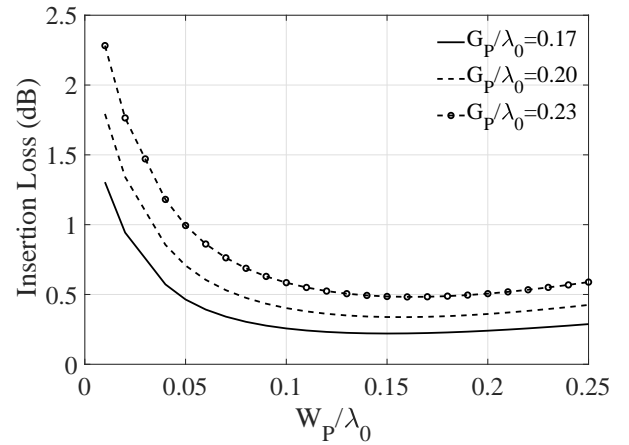
The objective of the synthesis for TA design is to realize a set of low-loss unit-cells attaining equispaced transmission phases. The procedure that we propose leverages on the model presented in Section II. It aims at determining the admittance tensors of the rotator sheets necessary to minimize the insertion loss of the unit-cells and cover the full phase range.

Since the synthesis focuses on the rotator, it is important to assess the impact of the other unit-cell elements, i.e. the dielectric spacers and the polarization grids, on the performance and derive some guidelines for their design. To this end, the variation of the transmission bandwidth is studied by performing fast parametric computations based on the analysis model, presented in Section II.

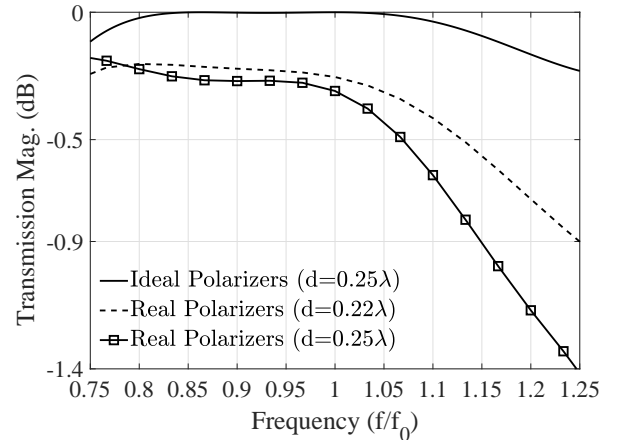
First, the effect of the spacers is investigated assuming that the outer sheets are ideal polarization grids. The transmission coefficient  $T^{yx}$  is calculated as a function of  $Y_u$  and  $Y_v$  using (5), for several values of the permittivity  $\epsilon_r$  and the thickness  $d$  of the spacers, at the design frequency  $\omega_0$ . For each of these values, the locus of the rotator admittances achieving perfect transmission is found. Then, the pair  $(Y_{u0}, Y_{v0})$  providing a specific value of the unit-cell transmission phase ( $90^\circ$  in this example) is selected. The rotator is assumed non-resonant. It is modeled as a pure inductance and a pure capacitance when excited by a  $u$ - and  $v$ -polarized wave, respectively. Assuming



(a)



(b)



(c)

Fig. 5: (a) 1-dB relative bandwidth (in %) of the unit-cell as a function of thickness and permittivity of the spacers. (b) Minimum insertion loss of the unit-cell as a function of the strip width,  $W_P$ , for three values of the gap,  $G_P$ . (c) Transmission coefficient (magnitude) as a function of frequency considering ideal and real polarizers.

without loss of generality that  $Y_{u0} > 0$  and  $Y_{v0} < 0$ , the equivalent capacitance and inductance are

$$C_0 = \frac{\Im\{Y_{u0}\}}{\omega_0}, \quad (15a)$$

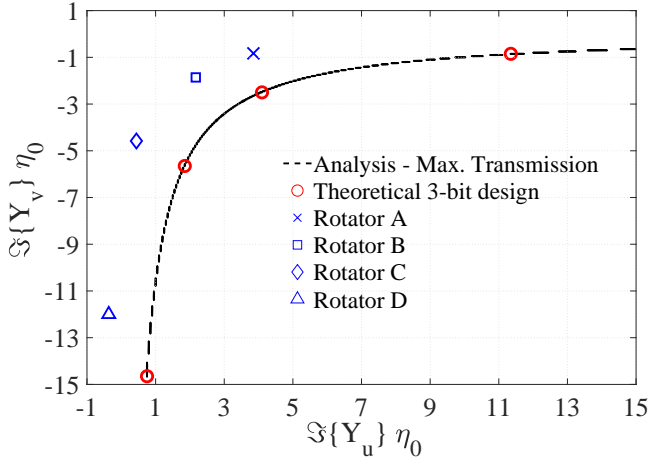


Fig. 6: Results of the synthesis procedure of the 3-bit TA at 300 GHz. By solving the expression (5) for maximum transmission, the dashed curve is derived. Assuming a 3-bit phase quantization, only four admittance pairs are needed (red circles), due to symmetry. The final results of the four rotators of Fig. 7 are depicted with blue symbols.

$$L_0 = \frac{-1}{\omega_0 \Im\{Y_{v0}\}}. \quad (15b)$$

Under this hypothesis, the frequency behavior of  $T^{yx}$  is determined. The computed 1-dB transmission bandwidth is plotted as a function of  $d$  and  $\epsilon_r$  in Fig. 5. The unit-cell is able to attain almost 100% relative bandwidth when exhibiting approximately quarter-wavelength spacing and a permittivity less than 4. This result is in agreement with previous designs in the literature [17], proving that the structure is considered very broadband.

The effects of the polarization grids can be studied using a similar procedure. It turns out that the behavior of a grid approaches that of an ideal polarizer as its period decreases [22], [23]. Nevertheless, even for relatively large periods, the mismatch introduced by the real grids with respect to ideal polarizers can be made very small with an appropriate choice of the filling factor  $\rho = W_P / (W_P + G_P)$ , where  $W_P$  is the strip width and  $G_P$  is the gap. As shown in Fig. 5b, in order to minimize the insertion loss of the unit-cell, the filling factor should be in the range between 0.2 and 0.4, when the gap is kept at a relatively small value. As an example, a grid with a period of  $\lambda_0/4$  and  $\rho = 0.32$  is selected, giving  $W_P = 0.08\lambda_0$  when  $G_P = 0.17\lambda_0$ . This choice not only minimizes the insertion loss, but also takes into account the fabrication constraints, as it will be discussed later. The sheet admittances of the chosen grid, simulated at the interface between vacuum and a dielectric of permittivity  $\epsilon_r = 3$ , are  $Y_t = j0.3/\eta_0$  and  $Y_r = -j5.4/\eta_0$ , at the center frequency  $f_0$ . The transmission coefficient of the unit-cell is plotted in Fig. 5c as a function of frequency, for ideal and actual polarization grids, when  $\epsilon_r = 3$ . The admittance tensor of the rotator is the same that has been considered to calculate the bandwidth in Fig. 5a, for  $\epsilon_r = 3$  and  $d = \lambda/4$ . The loading effect of the polarization grids introduces a small frequency shift of transmission coefficient. It can be compensated by slightly reducing the thicknesses of the spacers. By choosing  $d = 0.22\lambda$ , the frequency behavior of

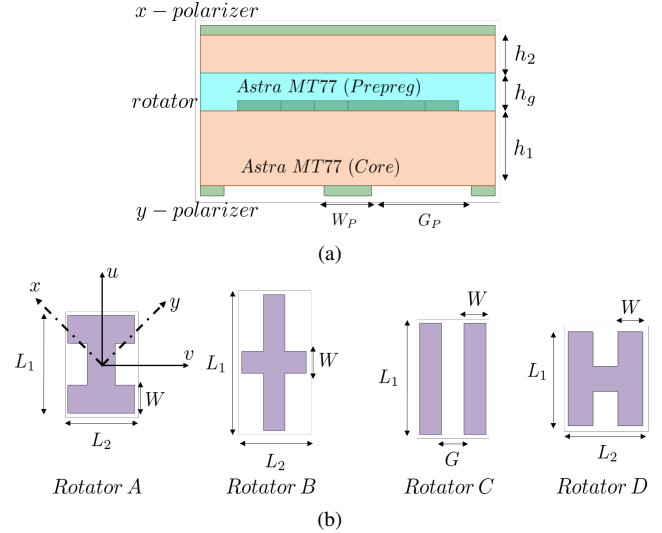


Fig. 7: (a) Stack-up of the unit-cells. (b) Rotator designs for the proposed 3-bit TA, in the  $(u, v)$  reference system (see Fig. 2). By mirroring each rotator with respect to the  $x$ -axis, the remaining four unit-cells are designed.

TABLE I: Geometrical parameters of the employed rotators.

Layer	Parameter (mm)			
	$L_1$	$L_2$	$W$	$G$
Rotator A	0.35	0.24	0.1	-
Rotator B	0.5	0.24	0.08	-
Rotator C	0.4	-	0.08	0.08
Rotator D	0.24	0.3	0.08	-

the unit-cell with real polarization grids matches the reference one obtained for ideal polarizers. The insertion loss at  $f_0$  is only 0.25 dB, determined by a slight mismatch due to the introduction of the polarization grids.

Next, the synthesis of the admittance tensor of the rotator is illustrated with applications to the design of a 3-bit TA operating at 300 GHz. Based on the previous parametric analysis and to ease the TA fabrication in PCB technology, the thicknesses and relative permittivity of the spacers are fixed to  $d = 0.22\lambda$  and  $\epsilon_r = 3$ , respectively, while the geometrical parameters of the grids are set to  $W_P = 0.08\text{mm}$  and  $G_P = 0.17\text{mm}$ . First, the transmission coefficient of the unit-cell is calculated as a function of  $Y_u$  and  $Y_v$  using (5) at the design frequency, similarly to what has been discussed in Fig. 4. Then, the locus of admittance values maximizing  $|T^{yx}|$  is numerically found. Finally,  $2^N$  admittance pairs  $(Y_u^i, Y_v^i)$ , with  $i = 1, \dots, 2^N$ , are selected on this locus to design unit-cells achieving a uniform  $N$ -bit quantization of the full phase range. The locus found for the 300-GHz design under analysis is plotted in Fig. 6. The pairs of rotator admittances selected to design 8 different unit-cells for a 3-bit TA are indicated with red circles. By virtue of symmetry, only the branch of the locus in the fourth quarter and four admittance pairs are shown.

The stack-up selected for the unit-cell design is shown in Fig. 7a. It comprises two Astra MT77 substrates and a bonding layer which have nominal permittivity equal to the targeted one ( $\epsilon_r = 3$ ) and are low-loss ( $\tan \delta = 0.0017$ ). The thicknesses

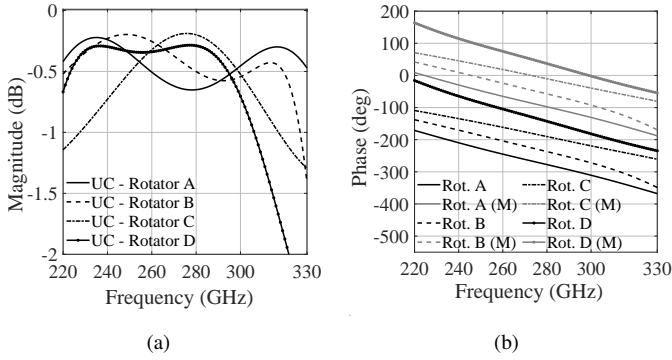


Fig. 8: Transmission magnitude (a) and phase (b) of the designed unit-cells, obtained from full-wave simulations. The results when the rotators of Fig. 7 are mirrored (M) with respect to  $x$ -axis are shown in dashed lines.

$h_1 = 0.127\text{mm}$  and  $h_2 = h_g = 0.064\text{mm}$  are chosen to get the desired spacer thickness ( $d = 0.22\lambda$ ) at 300 GHz. A key goal of this work was to make the design suitable for standard and low-cost PCB manufacturing. This requirement imposed to use conductor width and spacing larger than  $80\mu\text{m}$ . To overcome these strict constraints and achieve the targeted admittance pairs, four different rotator designs were employed. They are shown in Fig. 7 and their main dimensions are reported in Table I. All unit-cells are square. Their edge is  $P = \lambda_0/2 = 0.5\text{mm}$  to ensure that grating lobes do not occur and, at the same time, to ease the integration of controllable devices for future reconfigurable TA designs [30].

The sheet admittances of the four rotators of Fig. 7 at 300 GHz are shown with blue symbols in Fig. 6. They have been extracted from full-wave simulations performed in Ansys Electronic Desktop [19], [29]. Despite the technological constraints, the admittances of the designed rotators are very close to the targeted values obtained from the synthesis procedure. The phase error is less than  $5^\circ$  for each design, compared to the targeted value. These results prove the effectiveness of the proposed unit-cell design and synthesis procedure for the realization of low-cost TAs, even at sub-THz frequencies. The remaining four unit-cells are easily obtained by mirroring the rotators with respect to the  $x$ -axis. By virtue of symmetry, the admittances of the mirrored rotators approach the branch of the optimal admittance locus in the second quadrant (see Fig. 4). The transmission coefficient of each unit-cell with mirrored rotator is equal in magnitude but shifted in phase by  $180^\circ$  with respect to the corresponding original design.

Finally, the magnitude and phase of the transmission coefficients of all unit-cells, simulated under normal incidence and enforcing period boundaries, are shown in Fig. 8. The common 1-dB transmission bandwidth is almost 85 GHz, or 30% at the center frequency of 280 GHz. Over this band, the relative phase shifts among adjacent phase states are very close to  $45^\circ$ , with maximum absolute variations of  $10^\circ$ .

#### IV. TRANSMITARRAY DESIGN

Using the synthesized unit-cells, a  $40 \times 40$  elements ( $20\lambda_0 \times 20\lambda_0$ ) TA, with  $D = 20\text{mm}$ , is designed. The center

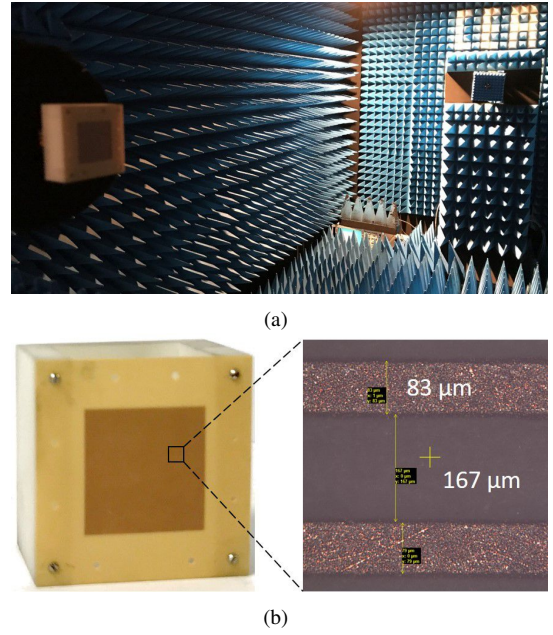


Fig. 9: (a) Measurement setup in the anechoic chamber and (b) view of the fabricated antenna prototype.

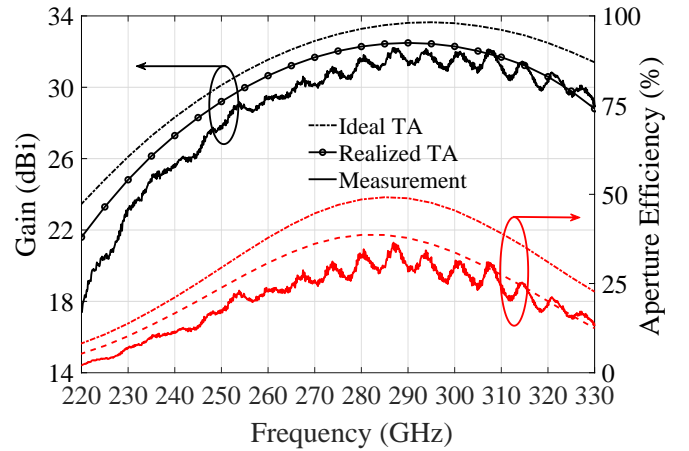


Fig. 10: Simulated and measured gain and aperture efficiency of the TA antenna prototype. The results are compared to an antenna comprising a perfect lens, considering the same focal source and focal distance.

frequency is 280 GHz at the range of observation. The aperture is illuminated by a 10-dBi horn (model 32240-10 by Flann Microwave) used as a focal source. The aperture of the horn has a size of  $1.31 \times 0.95\text{mm}^2$  and it is fed by a WR3 type waveguide. The optimal phase distribution is derived numerically by a hybrid simulation tool [1], employing the radiation pattern of the focal source and the simulated directivity and scattering parameters of the previous unit-cells. The focal distance was set at  $F = 20\text{mm}$  ( $F/D = 1$ ) in order to optimize the antenna in bandwidth and maintain a high aperture efficiency. The TA antenna was measured in the mm-wave anechoic chamber of CEA-Leti, as shown in Fig. 9a. A plastic support was used to fix the lens at the selected distance from the horn. The peak gain and aperture efficiency

TABLE II: Comparison with state-of-the-art transmitarrays at sub-THz frequencies.

Reference	[31]	[3]	[16]	[17]	<b>This work</b>
Frequency (GHz)	140	145	250	330	<b>300</b>
Technology	LTCC	PCB	PCB	PCB	<b>PCB</b>
No. layers	7	3	2	3	<b>3</b>
Vias	Yes	Yes	No	No	<b>No</b>
Feed gain (dBi)	20	10	6	7.7	<b>10</b>
TA size ( $\lambda_0^2$ )	18.67 $\times$ 18.67	20 $\times$ 20	14 $\times$ 14	11.67 $\times$ 11.67	<b>20<math>\times</math>20</b>
F/D	1.87	0.75	0.3	0.34	<b>1</b>
Peak gain (dBi)	33.5	33	28.8	23.1	<b>32.2</b>
Aperture efficiency (%)	50.1	38.3	32	12	<b>36.5</b>
Gain bandwidth (%)	10.7 (1-dB)	11.7 (1-dB)	6.8 (1-dB)	17.2 (3-dB)	<b>10.5 (1-dB)</b> <b>25.1 (3-dB)</b>

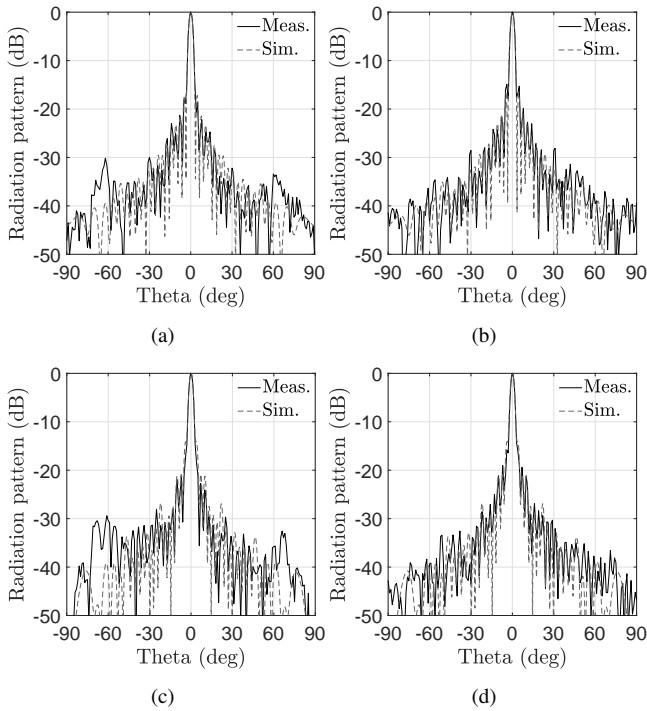


Fig. 11: Simulated and measured radiation pattern of the TA. (a) H-plane@280GHz, (b) E-plane@280GHz, (c) H-plane@300GHz and (d) E-plane@300GHz.

of the antenna prototype, as a function of frequency, are shown in Fig. 10. The maximum measured gain is 32.2 dBi at 287 GHz, with an aperture efficiency of 36.5%. The antenna attains approximately 29.3 GHz of 1-dB bandwidth and 70.4 GHz of 3-dB bandwidth, which are 10.5% and 25.1% at 280 GHz, respectively. The aperture efficiency is equal or greater than 24% between 265 and 310 GHz. The gain loss with respect to an ideal TA, i.e. reflectionless and providing perfect phase compensation, is only about 1.9 dB in the 3-dB bandwidth.

Finally, the radiation pattern at two frequencies is shown in Fig. 11 (H- and E-plane cuts). The simulated and measured results of the patterns are in good agreement and the maximum sidelobe level is about -19 dB and -15 dB in the H- and E-plane, respectively. Table II compares the performance of the antenna prototype to state-of-the-art transmitarrays at frequencies beyond 100 GHz. Compared to the designs in [16], [17]

an improvement of the aperture efficiency and the bandwidth are shown, while the antenna exhibits a larger electric size. The TA is via-less, comprising only 3 layers, realized using a low-cost technology.

## V. CONCLUSION

A new approach for analyzing and designing three-layer TAs comprising two outer orthogonal linear polarizers and an inner polarization rotator, has been presented and experimentally validated. A closed-form expression for the transmission coefficient of the unit-cell has been found by modeling it as three cascaded sheet admittances interleaved by two dielectric spacers. A four-port equivalent circuit has been derived to accurately describe the anisotropic behavior of the unit-cell and to ease its physical design. It has been rigorously demonstrated that the selected anisotropic unit-cell can achieve at the design frequency both nearly perfect transmission and full phase coverage, as opposed to standard symmetric FSS designs. It has been shown that, following proper design guidelines, the transmission phase can be tuned by varying the inner sheet only. Based on this observation, a procedure to synthesize the admittance tensor of the inner layer and realize multiple low-loss TA unit-cells has been proposed. It requires the optimization of only two admittance parameters.

With this approach, a 3-bit 40 $\times$ 40 TA at 300 GHz was designed, using standard vialess PCB technology. Despite the strict fabrication constraints, the admittances of the designed unit-cells approach the targeted values, proving the effectiveness and robustness of the proposed design procedure. The simulated insertion loss of all unit-cells is less than 1-dB between 230 and 315 GHz. The TA has been optimized for a 10-dBi horn feed and F/D = 1. The prototype outperforms state-of-the-art TA antennas operating at frequencies higher than 200 GHz and fabricated in PCB technology. The measured peak gain and relative 3-dB bandwidth are 32.2 dBi and 25.1%, respectively. The aperture efficiency reaches a maximum value of 36.5% at 287 GHz. These results and the low-cost fabrication technology pave the way for the integration of the proposed TA design in future sub-THz wireless systems.

## APPENDIX

The scattering parameters of the four-port circuit in Fig. 2 are calculated using classical network theory [27]. In this

paper, the main interest is on the properties of the transmission coefficient  $S_{31}$ . In order to derive its expression, the ports 2, 3 and 4 must be terminated with matched loads, equal to  $Z_0$ . Then, the relation between transmitted and incident waves,  $V_3^-$  and  $V_1^+$ , respectively, is derived. By doing so, the parameter  $K_1$  in (5) is found to be

$$K_1 = Z_{\varepsilon_r}^{-1}(1 - \Gamma_2) - Y_A(1 + \Gamma_2) - Z_{P2}^{-1}(1 + \Gamma_2) \quad (16)$$

The impedance  $Z_{P2}$  in (16) is equal to

$$Z_{P2} = Z_{\varepsilon_r} \frac{Z_{L1} + jZ_{\varepsilon_r} \tan(\beta d_2)}{Z_{\varepsilon_r} + jZ_{L1} \tan(\beta d_2)}, \quad (17)$$

where

$$Z_{L1} = \frac{Z_0}{1 + Z_0 Y_r} \quad (18)$$

The coefficient  $\Gamma_1$  is equal to

$$\Gamma_1 = \frac{Z_{L2} - Z_{\varepsilon_r}}{Z_{L2} + Z_{\varepsilon_r}}, \quad (19)$$

where

$$Z_{L2} = \frac{Z_0}{1 + Z_0 Y_t} \quad (20)$$

The coefficient  $\Gamma_2$  is equal to

$$\Gamma_2 = \frac{Z_{in}^{BB'} - Z_{\varepsilon_r}}{Z_{in}^{BB'} + Z_{\varepsilon_r}} \quad (21)$$

The parameter  $Z_{in}^{BB'}$  is the input impedance at  $BB'$ , seen as the equivalent load of the first transmission line of Port 1. Similarly, the parameter  $K_2$  can be found as

$$K_2 = \frac{(Y_B + Y_{in}^{EE'})(e^{j\beta d_2} + \Gamma_1 e^{-j\beta d_2})(e^{j\beta d_1} - \Gamma_2 e^{-j\beta d_1})}{Z_{\varepsilon_r}(1 + \Gamma_1)} \quad (22)$$

The admittance  $Y_{in}^{EE'}$  in (22) is the equivalent input admittance at  $EE'$ , including Ports 3 and 4, seen by the rest of the circuit.

## REFERENCES

- [1] H. Kaouach, L. Dussopt, J. Lanteri, T. Koleck, and R. Sauleau, "Wideband low-loss linear and circular polarization transmit-arrays in V-band," *IEEE Trans. Antennas Propag.*, vol. 59, no. 7, pp. 2513–2523, Jul. 2011.
- [2] C. Jouanlanne, A. Clemente, M. Huchard, J. Keignart, C. Barbier, T. Le Nadan, and L. Petit, "Wideband linearly polarized transmitarray antenna for 60 GHz backhauling," *IEEE Trans. Antennas Propag.*, vol. 65, no. 3, pp. 1440–1445, Jan. 2017.
- [3] F. Foglia Manzillo, A. Clemente, and J. L. González-Jiménez, "High-Gain D-band transmitarrays in standard PCB technology for beyond-5G communications," *IEEE Trans. Antennas Propag.*, vol. 68, no. 1, pp. 587–592, Jan. 2020.
- [4] C. Pfeiffer and A. Grbic, "Millimeter-wave transmitarrays for wavefront and polarization control," *IEEE Trans. Microw. Theory Techn.*, vol. 61, no. 12, pp. 4407–4417, Dec. 2013.
- [5] A. H. Abdelrahman, A. Z. Elsherbeni, and F. Yang, "Transmitarray antenna design using cross-slot elements with no dielectric substrate," *IEEE Antennas Wireless Propag. Lett.*, vol. 13, pp. 177–180, Jan. 2014.
- [6] Q. Luo, S. Gao, M. Sobhy, and X. Yang, "Wideband transmitarray with reduced profile," *IEEE Antennas Wireless Propag. Lett.*, vol. 17, no. 3, pp. 450–453, Mar. 2018.
- [7] S. L. Liu, X. Q. Lin, Z. Q. Yang, Y. J. Chen, and J. W. Yu, "W-band low-profile transmitarray antenna using different types of FSS units," *IEEE Trans. Antennas Propag.*, vol. 66, no. 9, pp. 4613–4619, Sept. 2018.
- [8] P. Feng, S. Qu, and S. Yang, "Octave bandwidth transmitarrays with a flat gain," *IEEE Trans. Antennas Propag.*, vol. 66, no. 10, pp. 5231–5238, Oct. 2018.
- [9] Y. Ge, C. Lin, and Y. Liu, "Broadband folded transmitarray antenna based on an ultrathin transmission polarizer," *IEEE Trans. Antennas Propag.*, vol. 66, no. 11, pp. 5974–5981, Nov. 2018.
- [10] P. Feng and S. Qu, "60-GHz 2D scan phased transmitarray with high gain and low profile," in *13th Eur. Conf. Antennas Propag. (EuCAP)*, Krakow, Poland, Mar. 2019, pp. 1–4.
- [11] K. Mavrakakis, H. Luyen, J. H. Booske, and N. Behdad, "Wideband transmitarrays based on polarization-rotating miniaturized-element frequency selective surfaces," *IEEE Trans. Antennas Propag.*, vol. 68, no. 3, pp. 2128–2137, Mar. 2020.
- [12] P. Mei, G. F. Pedersen, and S. Zhang, "A broadband and FSS-based transmitarray antenna for 5G millimeter-wave applications," *IEEE Antennas Wireless Propag. Lett.*, vol. 20, no. 1, pp. 103–107, Jan. 2021.
- [13] K. Xu, Z. Xiao, J. Tang, D. Liu, and Z. Wang, "Ultra-broad band and dual-band highly efficient polarization conversion based on the three-layered chiral structure," *Physica E*, vol. 81, pp. 169–176, 2016.
- [14] Y. Cheng, R. Gong, and L. Wu, "Ultra-broadband linear polarization conversion via diode-like asymmetric transmission with composite meta-material for terahertz waves," *Plasmonics*, vol. 10, no. 12, pp. 1113–1120, Aug. 2017.
- [15] J.-S. Li and F.-Q. Bai, "Dual-band terahertz polarization converter with high-efficiency asymmetric transmission," *Opt. Mater. Express*, vol. 10, no. 8, pp. 1853–1861, Aug. 2020.
- [16] S. Qu and H. Yi, "Low-cost two-layer terahertz transmitarray," *Int. Appl. Comput. Electromagn. Soc. Symp. (ACES)*, pp. 1–2, Aug. 2017.
- [17] K. Medrar, L. Marnat, L. Dussopt, C. Belem-Goncalves, G. Ducournau, C. Luxey, and F. Giancesello, "H-band substrate-integrated discrete lens antenna for high data rate communication systems," *IEEE Trans. Antennas Propag. (Early Access)*, Dec. 2020.
- [18] O. Koutsos, F. Foglia Manzillo, A. Clemente, and R. Sauleau, "Design of a 3-bit transmitarray antenna at 300 GHz using asymmetric linear polarizers," in *IEEE Int. Symp. Antennas Propag. (APS/URSI)*, Montreal, QC, Canada, Jul. 2020, pp. 1505–1506.
- [19] C. Pfeiffer and A. Grbic, "Bianisotropic metasurfaces for optimal polarization control: Analysis and synthesis," *Phys. Rev. Applied*, vol. 2, p. 044011, Oct. 2014.
- [20] O. Koutsos, F. Foglia Manzillo, A. Clemente, and R. Sauleau, "Analysis and efficient design of sub-THz transmitarrays with three anisotropic layers," in *15th Eur. Conf. Antennas Propag. (EuCAP)*, Dusseldorf, Germany, Mar. 2021, pp. 1–5.
- [21] A. H. Abdelrahman, A. Z. Elsherbeni, and F. Yang, "Transmission phase limit of multilayer frequency-selective surfaces for transmitarray designs," *IEEE Trans. Antennas Propag.*, vol. 62, no. 2, pp. 690–697, Feb. 2014.
- [22] R. Sauleau, P. Coquet, J. P. Daniel, T. Matsui, and N. Hirose, "Study of Fabry-Perot cavities with metal mesh mirrors using equivalent circuit models. Comparison with experimental results in the 60 GHz band," *J. Infrared Millim Waves*, vol. 19, no. 12, pp. 1693–1710, Dec. 1998.
- [23] R. Sauleau, D. Thouroude, P. Coquet, and J. P. Daniel, "Theoretical reflection coefficient of metal grid reflectors at a dielectric boundary," *J. Infrared Millim Waves*, vol. 20, no. 2, pp. 325–340, Feb. 1999.
- [24] M. Ando and Ken Takei, "Reflection and transmission coefficients of a thin strip grating for antenna application," *IEEE Trans. Antennas Propag.*, vol. 35, no. 4, pp. 367–371, Apr. 1987.
- [25] N. Marcuvitz, *Waveguide Handbook*. GBR: Institution of Electrical Engineers, 1986.
- [26] M. Selvanayagam and G. V. Eleftheriades, "Discontinuous electromagnetic fields using orthogonal electric and magnetic currents for wavefront manipulation," *Opt. Express*, vol. 21, no. 12, pp. 14 409–14 429, Jun. 2013.
- [27] D. M. Pozar, *Microwave engineering; 3rd ed.* Hoboken, NJ: Wiley, 2005.
- [28] A. M. Patel and A. Grbic, "Transformation electromagnetics devices based on printed-circuit tensor impedance surfaces," *IEEE Trans. Microw. Theory Techn.*, vol. 62, no. 5, pp. 1102–1111, May 2014.
- [29] M. Borgese and F. Costa, "A simple equivalent circuit approach for anisotropic frequency-selective surfaces and metasurfaces," *IEEE Trans. Antennas Propag.*, vol. 68, no. 10, pp. 7088–7098, Oct. 2020.
- [30] C. W. Luo, G. Zhao, Y. C. Jiao, G. T. Chen, and Y. Yang-Dong, "Wideband 1-bit reconfigurable transmitarray antenna based on polarization rotation element," *IEEE Antennas Wireless Propag. Lett.*, vol. 20, no. 5, pp. 798–802, Mar. 2021.
- [31] Z. Miao, Z. Hao, G. Q. Luo, L. Gao, J. Wang, X. Wang, and W. Hong, "140 GHz high-gain LTCC-integrated transmit-array antenna using a wideband SIW aperture-coupling phase delay structure," *IEEE Trans. Antennas Propag.*, vol. 66, no. 1, pp. 182–190, Jan. 2018.



**Orestis Koutsos** received the Diploma degree in electrical and computer engineering from the Aristotle University of Thessaloniki, Thessaloniki, Greece, in 2017. He is currently pursuing the Ph.D. degree in signal processing and telecommunications with the University of Rennes 1, France and CEA Leti, Grenoble, France. His current research interests include the analysis, synthesis, and design of transmitarray antennas, and the numerical modeling of antenna arrays and periodic structures.

Mr. Koutsos was finalist of a paper shortlisted for the Best Student Paper Award at the 15th European Conference on Antennas and Propagation in 2021.



**Francesco Foglia Manzillo** (Member, IEEE) received the B.Sc. and M.Sc. degrees (cum laude) in electronics engineering from the University of Naples Federico II, Naples, Italy, in 2010 and 2012, respectively, and the Ph.D. degree in signal processing and telecommunications from the University of Rennes 1, Rennes, France, in 2017. In 2012, he was an Intern at the Electronic Research Laboratory, Delft University of Technology, Delft, The Netherlands, and at NXP Semiconductors, Eindhoven, The Netherlands. In 2016, he spent six months as a Visiting Ph.D. Student at the Radiation Laboratory, University of Michigan, Ann Arbor, MI, USA. Since July 2017, he has been with the French Alternative Energies and Atomic Energy Commission, Laboratory of Electronics and Information Technologies (CEA-Leti), Grenoble, France.

His research interests include the analysis, synthesis, and design of antenna arrays, quasi-periodic structures (e.g. transmitarrays and polarization converters), numerical modeling, beamforming systems, and the integration of millimeter-wave radio systems.

Dr. Foglia Manzillo was a co-recipient of the Best Innovation Award at the 39th European Space Agency Antenna Workshop in 2018 and co-authored a paper shortlisted for the Best Student Paper Award at the 15th European Conference on Antennas and Propagation in 2021.



**Antonio Clemente** (S'11 - A'13 - M'14 - SM'17) received the B.S. and M.S. degrees in telecommunication engineering and remote sensing systems from the University of Siena, Italy, in 2006 and 2009, respectively, the Ph.D. degree in signal processing and telecommunications, and the "Habilitation à Diriger des Recherches" degree from the University of Rennes 1, France, in 2012 and 2021, respectively. From October 2008 to May 2009, he realized his master thesis project at Technical University of Denmark (DTU), Lyngby, Denmark, where he

worked on spherical near-field antenna measurements. His Ph.D. project has been realized at CEA Leti, Grenoble, France. In 2012, he joined the R&D laboratory of Satimo Industries, Villebon-sur-Yvette, France. Since 2013, he is a Research Scientist at CEA Leti, Grenoble, France.

His current research interests include fixed-beam and electronically reconfigurable transmitarray antennas, millimeter-wave and sub-THz Antenna-in-Package (AiP), antenna arrays, periodic or quasi-periodic structures, near-field focused systems, antenna theory and fundamental limitations, synthesis and modelling, and near-field and far-field antenna measurements. He has authored or co-authored more than 120 papers in international journals and conferences, and received 18 patents. He has been involved in more than 25 research projects at the national and European levels. From 2016 to 2018, he has been the technical coordinator of the H2020 joint Europe and South Korea 5GCHAMPION project.

Dr. Clemente serves as reviewer for the numerous IEEE and IET journals in the field of Microwave, Antennas and Propagation. He received the Young Scientist Award (First Prize) during the 15th International Symposium of Antenna Technology and Applied Electromagnetics (ANTEM 2012), the Best Antenna Design and Applications Paper Award during the 13th European Conference on Antennas and Propagation (EuCAP 2109). He is co-recipient of the Best Paper Award at JNM 2015 (19emes Journées Nationales Microondes) and of the 2019 ETRI Journal Best Paper Award. In 2019, he was a finalist for the "Microwave Prize" at the European Microwave Conference (EuMC 2019).



**Ronan Sauleau** (M'04 – SM'06 – F'18) graduated in electrical engineering and radio communications from the Institut National des Sciences Appliquées, Rennes, France, in 1995. He received the Agrégation degree from the Ecole Normale Supérieure de Cachan, France, in 1996, and the Doctoral degree in signal processing and telecommunications and the "Habilitation à Diriger des Recherches" degree, both from the University of Rennes 1, France, in 1999 and 2005, respectively. He was an Assistant Professor and Associate Professor at the University of Rennes

1, between September 2000 and November 2005, and between December 2005 and October 2009, respectively. He has been appointed as a full Professor in the same University since November 2009.

His current research fields are numerical modeling, millimeter-wave beam steering antennas, substrate integrated waveguide antennas, lens-based focusing devices, periodic and non-periodic structures (FSS, metasurfaces, polarizers, reflectarrays, and transmitarrays) and biological effects of millimeter waves.

He has been involved in more than 70 research projects at the national and European levels and has co-supervised 27 post-doctoral fellows, 57 PhD students and 50 master students.

He has received 20 patents and is the author or coauthor of more than 275 journal papers and 570 publications in international conferences and workshops. He was co-director of the research Department 'Antenna and Microwave Devices' at IETR and deputy director of IETR between 2012 and 2016. He is now director of IETR. Prof. Sauleau received the 2004 ISAP Conference Young Researcher Scientist Fellowship (Japan) and the first Young Researcher Prize in Brittany, France, in 2001 for his research work on gain-enhanced Fabry-Perot antennas. In September 2007, he was elevated to Junior member of the "Institut Universitaire de France". He was awarded the Bronze medal by CNRS in 2008, and the silver medal in 2020. He received the 2021 Antenna EurAAP Award. He was the co-recipient of several international conference awards with some of his students (Int. Sch. of BioEM 2005, BEMS'2006, MRRS'2008, E-MRS'2011, BEMS'2011, IMS'2012, Antem'2012, BioEM'2015, EuCAP'2019, EuCAP'2021). He served as a guest editor for the IEEE Antennas Propagat. Special Issue on "Antennas and Propagation at mm and sub mm waves". He served as a national delegate for several EU COST actions. He has served as a national delegate for EurAAP and as a member of the board of Director of EurAAP from 2013 to 2018.